Radiation Science and Technology
2025, Vol. 11, No. 1, pp. 1-11
https://doi.org/10.11648/j.rst.20251101.11

Research Article

Effect of Kernel Functions on the Performance of Support Vector Regression Algorithm in Predicting Patient-Specific Organ Doses from CT Scans

Wencheng Shao[1, 2, †], Xin Lin[1, †], Ying Huang[3], Liangyong Qu[4], Weihai Zhuo[1, *], Haikuan Liu[1, *]

[1]Institute of Radiation Medicine, Fudan University, Shanghai, China

[2]Department of Radiation Physics, Harbin Medical University Cancer Hospital, Harbin, China

[3]Department of Nuclear Science and Technology, Institute of Modern Physics, Fudan University, Shanghai, China

[4]Department of Radiology, Shanghai Zhongye Hospital, Shanghai, China

Abstract

Background: CT examinations are commonly utilized for the diagnosis of internal diseases. The X-rays emitted during CT scans can elevate the risks of developing solid cancers by causing DNA damage. The risk of CT scan-induced solid cancers is intricately linked to the organ doses specific to each patient. The Support Vector Regression (SVR) algorithm exhibits the capability to swiftly and accurately predict organ doses. Kernel functions, including linear, polynomial, and radial basis (RBF) functions, play a crucial role in the overall performance of SVR when predicting patient-specific organ doses from CT scans. Therefore, it is imperative to investigate the influence of kernel selection on the comprehensive predictive effectiveness of SVR. *Purpose:* This study investigates the impact of kernel functions on the predictive performance of SVR models trained by radiomics features, and to pinpoint the optimal kernel function for predicting patient-specific organ doses from CT scans. *Methods:* CT images from head and abdominal CT scans were processed using DeepViewer®, an auto-segmentation tool for defining regions of interest (ROIs) within their organs. Radiomics features were extracted from the CT data and ROIs. Benchmark organ doses were calculated through Monte Carlo simulations. SVR models, utilizing the radiomics features, were trained with linear-, polynomial-, and RBF kernels to predict patient-specific organ doses from CT scans. The robustness of the SVR prediction was examined by applying 25 random sample splits with each kernel. The mean absolute percentage error (MAPE) and coefficient of determination (R^2) were compared among the kernels to identify the optimal kernel. *Results:* The linear kernel obtains better overall predictive performance than the polynomial and RBF kernels. The SVR trained with the linear kernel function achieves lower MAPE values, below 5% for head organs and under 6.8% for abdominal organs. Furthermore, it shows higher R^2 values exceeding 0.85 for head organs and going beyond 0.8 for abdominal organs. *Conclusions:* Kernel selection severely impact the overall performance of SVR models. The optimal kernel varies with CT scanned parts and organ types indicating the necessity to conduct organ-specific kernel selection.

[*]Corresponding author: whzhuo@fudan.edu.cn (Weihai Zhuo)

[†]Xin Lin and Wencheng Shao are co-first authors.

Received: 11 February 2025; **Accepted:** 20 February 2025; **Published:** 21 March 2025

Keywords

CT, Organ Dose, SVR, Radiomics Features, Kernel Function

1. Introduction

Widely utilized for diagnostic purposes across various medical conditions, computed tomography (CT) has emerged as a valuable tool, providing detailed cross-sectional visuals of internal organs and tissue structures [1-4]. Its significance lies in the detection of an array of pathological conditions, encompassing infectious, traumatic, inflammatory, and hemorrhagic disorders [5-7]. Nonetheless, the administration of CT scans exposes patients to ionizing radiation, resulting in absorbed doses to vital organs. This radiation exposure has the potential to increase the risk of developing solid and hematological malignancies [8-11]. The necessity arises to predict patient-specific organ doses due to CT examinations.

At present, neural networks (NN) [12-15] has outperformed size-specific dose estimates (SSDE) [16-19] in terms of accuracy in predicting patient-specific organ dose from CT scans by considering a broader spectrum of patient characteristics. However, NN-based models might be sensitive to outliers that are not uncommon due to individual variations and anomalies in patient conditions, potentially compromising the model's overall performance. Besides, NN-based models may require huge amount of patient samples to achieve consistent and accurate predictive performance with variations in the patient dataset because of extensive parameterization. [20, 21]

In the realm of medical data, limitations often arise due to privacy constraints and the intricate nature of obtaining labeled data. [22, 23] Support Vector Regression (SVR) exhibits its obvious advantages in handling limited patient datasets. [24] SVR's straightforward structure and emphasis on pivotal support vectors render it more resistant to overfitting, ensuring dependable predictions even when dealing with constrained patient data. Additionally, SVR excels in its robustness to outliers, further increasing its advantage in achieving consistent performance across diverse patient datasets.

The kernel function is pivotal in SVR as it transforms input data into a higher-dimensional space, allowing the algorithm to capture complex patterns. [25] SVR relies on this function for non-linear regression by mapping data into a space where linear regression is effective. Choosing the appropriate kernel (linear, polynomial, radial basis, sigmoid) is crucial, impacting the model's ability to accurately generalize and predict on unseen dataset. A well-selected kernel enhances performance, while an inappropriate one can lead to poor results, emphasizing the critical role of the kernel in SVR for robust regression models.

To date, our previous study has investigated the predicted head organ doses with SVR models trained by radiomics features. [26] The study just employed a fixed kernel function, specifically the radial basis function (RBF). But, the study did not adopt kernel function selection as a crucial procedure in maximizing SVR's performance as much as possible. Thus, it is necessary to investigate the effect of kernel functions on SVR's performance in predicting patient-specific organ doses from CT scans so as to pinpoint the optimal kernel function for each organ. Unlike previous studies, this study respectively applied linear, polynomial, and RBF to train SVR-based patient-specific organ dose prediction models using radiomics features, and compared the regression metrics including mean absolute percentage error (MAPE) and the coefficient of determination (R^2), among the SVR models trained by the three kernel functions for each investigated organ. The optimal kernel function was selected as the one that made the SVR model achieve the highest R^2 and lowest MAPE.

2. Materials and Methods

2.1. Patient Data Collection and Input Data Processing

This study analyzed a substantial cohort of 237 head and 235 abdominal scans at Shanghai Zhongye Hospital. Employing the automated segmentation software traded with DeepViewer® [27], CT images were segmented to identify regions of interest (ROIs) encompassing vital anatomical structures. The segmented organs include brain, left eye, right eye, left lens, right lens, liver, left kidney, right kidney, and bowel. The delineation of ROIs facilitated radiomics feature extraction. For this purpose, acquired CT images and corresponding ROIs were transformed from Digital Imaging and Communications in Medicine (DICOM) to Neuroimaging Informatics Technology Initiative (NIFTI) format using the "dcmstruct2nii" tool [28]. This conversion is crucial for generating essential CT and mask data. Maintaining a standardized scan voltage of 120 kilo electronvolts (keV) across all examinations ensured uniformity in the imaging process, minimizing potential confounding factors in radiomics feature extraction and subsequent data analysis.

In this study, radiomics features were extracted from CT images and ROIs using the Pyradiomics module [29]. The process involved image preprocessing, feature computation,

and feature selection. During preprocessing, CT images and masks were spatially standardized through resampling to (1, 1, 3) for head scans, (1, 1, 5) for abdominal scans by setting the "resamplePixelSpacing" parameter. Data augmentation [25] was adopted to enhance the diversity of input radiomics features during SVR model training. For each organ, 107 radiomics features were extracted across seven categories, capturing aspects like correlation, homogeneity, and contrast within ROIs. The f-regression function was applied to identify the most relevant features by calculating and comparing F-value and p-value [31], indicating strong, significant linear relationships with the y values. The top 100 radiomics features were adopted as inputs to train the SVR-based organ dose prediction models. The extraction and selection were accomplished in the Anaconda 3 [32] environment with double AMD EPYC 7551 CPUs.

2.2. Benchmark Organ Dose

This study employed the GPUGeant4-based Monte Carlo Simulations (GGEMS) for precise and efficient computation of reference organ doses from CT images and masks. [33] GGEMS excels in managing complex geometries, diverse materials, and multiple radiation sources (photons and electrons), surpassing CPU-based MC simulation codes in speed and maintaining high precision. The GPU-calculated organ doses, achieved using Nvidia RTX4090 graphics cards, served as references for training SVR models to predict doses for seven organs. MC simulations with an error threshold below 2% per voxel ensured dependable organ dose estimations, considering the auto-tube current effect. This SVR-based approach, utilizing GGEMS, provides a reliable alternative to neural network models for predicting organ doses based on GPU-accelerated MC simulations.

2.3. Metrics for Assessing SVR Performance

We employed regression metrics such as MAPE and R^2. MAPE measures the mean absolute percentage disparities between real and predicted values, offering a gauge for the proximity of predictive outputs to actual values in percentage terms, irrespective of error direction. The expression for MAPE can be expressed as follows:

$$MAPE = \frac{1}{n}\sum_{i=1}^{n} \left| \frac{y_i - \hat{y}_i}{y_i} \right| \times 100\% \quad (1)$$

where n is the patient count, y_i represents the actual reference organ dose, and $\hat{y}_i$ denotes the anticipated organ dose. R^2 reveals the proportion of variance in the output variable attributed to the impact of input variables. Its primary function is to quantify the goodness-of-fit of the regression model to the dataset, with a higher R^2 value indicating a more effective model fit. The mathematical expression for R^2 is as follows:

$$R^2 = 1 - \frac{\sum_{i=1}^{n}(y_i - \hat{y}_i)^2}{\sum_{i=1}^{n}(y_i - \bar{y})^2} \quad (2)$$

2.4. SVR Algorithm and Kernel Function Selection

SVR, a potent machine learning algorithm in the support vector machines (SVMs) family, differs from traditional regression models by prioritizing control over the margin of error. It excels in handling complex and nonlinear relationships between input variables and output. Built on SVM principles for classification, SVR extends them to regression, aiming to find a hyperplane that optimally captures this relationship. Utilizing a kernel trick, SVR can map input features into a higher-dimensional space, facilitating the capture of intricate patterns. This flexibility makes SVR well-suited for various real-world regression problems, particularly those involving nonlinear relationships. Its inherent robustness to outliers, courtesy of the margin concept, renders SVR effective for datasets with noisy or irregular patterns.

Kernel functions will influence the interpretation of SVR and modelling the underlying relationships among the data. Different kernel functions have various effects on the shape and flexibility of the hyperplane that SVR seeks to find in the transformed feature space. SVR uses various kernel functions including linear, polynomial, and RBF kernel to map the input data into a higher-dimensional space, enabling the algorithm to capture complex relationships. The linear kernel represents a simple dot product between the input features, preserving linear relationships. It is suitable when the underlying relationship between variables is assumed to be linear. Its mathematical expression can be written as:

$$K(x, x') = x \bullet x' \quad (3)$$

where x and x' stand for the input data and mapped data, respectively. The polynomial kernel introduces non-linearity by computing a polynomial function of degree d of the dot product between input features, where c is a constant. It is capable of capturing polynomial relationships between variables. Its mathematical expression can be written as:

$$K(x, x') = (x \cdot x' + c)^d \quad (4)$$

The RBF kernel, also known as the Gaussian kernel, introduces a non-linear transformation based on the radial distance between data points. The parameter γ determines the width of the radial basis function and influences the flexibility of the decision boundary. It is effective in capturing complex, non-linear relationships. Its mathematical expression can be written as:

$$K(x, x') = exp(-\gamma \cdot \| x - x' \|^2) \quad (5)$$

The choice of kernel function can significantly impact SVR's performance, especially when dealing with datasets exhibiting nonlinear relationships. The selection of a kernel function in SVR is crucial as it determines the transformation applied to the input features, allowing SVR to capture complex relationships between variables. The kernel function essentially serves as a mathematical technique to implicitly map the input features into a higher-dimensional space, making it possible to identify and model intricate patterns that may not be apparent in the original feature space.

As shown in Fig. 1, we employed three prediction models for estimating patient-specific organ doses using SVR for each organ. These models, labeled as SVR_1, SVR_2, and SVR_3, were trained with distinct kernels: linear, polynomial, and RBF. To assess the reliability of each SVR model, we conducted 25 random patient sample splits, maintaining an 80:20 ratio between the training set and test set. We then calculated the mean and standard deviation of regression metrics (MAPE and R^2) for SVR_1, SVR_2, and SVR_3. The optimal kernel was identified as the one that resulted in the SVR model achieving the highest R^2 and the mean MAPE. We trained the SVR prediction models by using the Scikit-learn module when setting the regulation parameter (C value) as 5. Referring to equations 4 and 5, we employed the default values for *'c'* (set to 0) and *'d'* (set to 3) as specified in the Scikit-learn module, and the γ value was automatically calculated as the reciprocal of the total number of input radiomics features during the training of SVR using the Scikit-learn module.

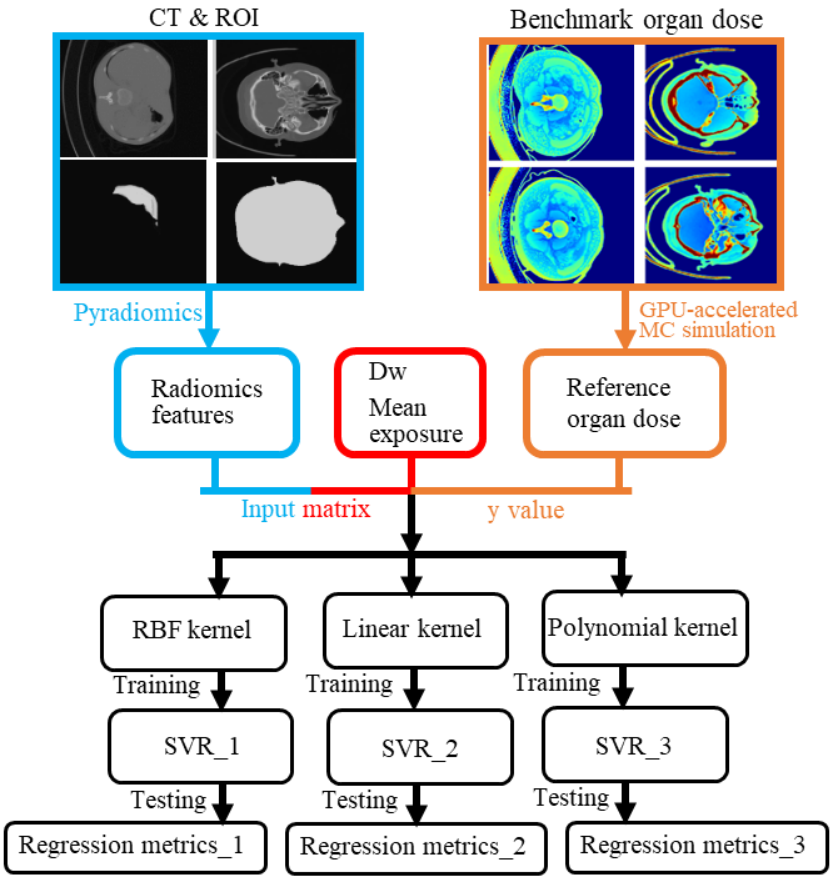

Figure 1. *General workflow for selecting the kernel functions and constructing optimal SVR models for predicting patient-specific organ doses for head and abdominal patients.*

3. Results

In this study, we evaluated the performance of the trained SVR model for each investigated organ, including the brain, left eye, right eye, left lens, right lens, liver, left kidney, right kidney, and bowel. The results, presented in subsections 3.1 and 3.2, consist of the MAPE and R^2 values, respectively, obtained from 25 random patient sample splits. Box chart plots were adopted to depict the overall performance accompanying the robustness, which revealed the SVR-based model's predictive stability against patient sample variations. Figures 2 and 3 show the regression metrics of the head organs and abdominal organs, respectively.

In Figures 2 and 3, each box chart plot displays a chart where the central box signifies the interquartile range (IQR), spanning from the first quartile (Q1) to the third quartile (Q3). The lower and upper edges of the box correspond to the 25th

percentile (Q1) and 75th percentile (Q3) of the dataset, respectively. The box's length visually represents the dispersion of the central 50% of the data. Inside the box, a horizontal line denotes the median, which is the middle value in an ordered dataset. The median serves as a robust measure of central tendency, unaffected by extreme values, providing insight into the distribution's center. The empty square in the box chart represents the mean. Whiskers extend from the box edges, indicating the data range. The lower whisker reaches the minimum data point of the 1st percentile. The upper whisker reaches the maximum data point of the 99th percentile.

3.1. Regression Metrics for the Head Organs

As shown in Figures 2a and 2b for the brain, the mean values of MAPE across 25 random sample splits are 1.3%, 1.6%, and 2.0%, and the mean values of R^2 are 0.9, 0.85, and 0.8 for the linear, polynomial, and RBF kernels, respectively. This suggests that SVR-based model with the linear kernel shows the best overall performance in both accuracy and generality in predicting patient-specific brain doses. For the left lens (see Figure 2h), there are few predictive data points with the values of R^2 smaller than 0.5, indicating a slightly low robustness in predictive generality across diverse patient sample splits for the linear kernel, but this did not lead the obvious compromising in MAPE. This suggests the linear kernel-based SVR's predictive performance is hardly to be deteriorated by patient sample allocation in prediction brain doses. Thus, to utilize the high overall performance from applying the linear kernel to train SVR models, the robustness in R^2 across multiple patient sample splits should be verified to discard the rare splits with worse regression metrics, and to pinpoint the appropriate sample split strategies.

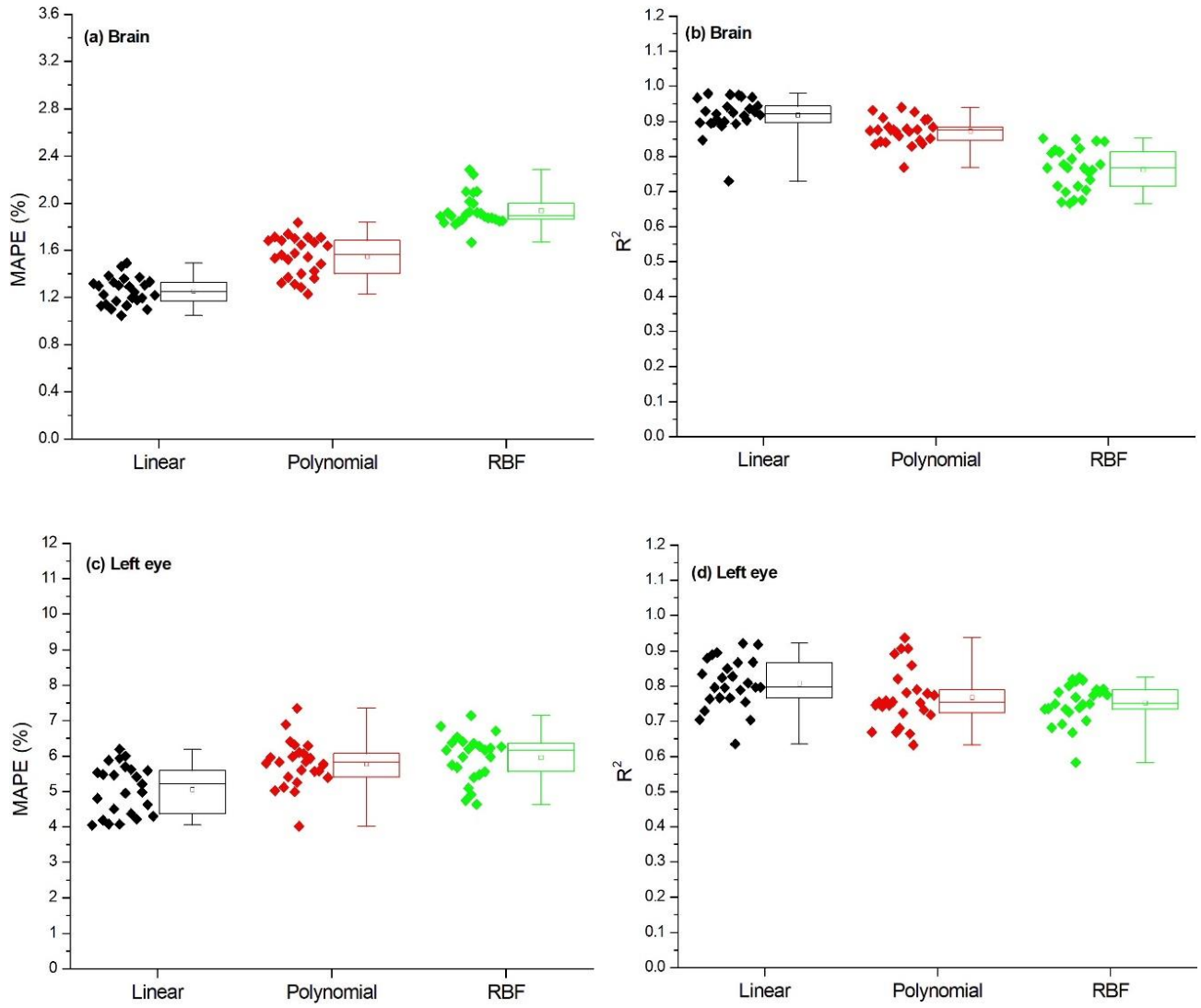

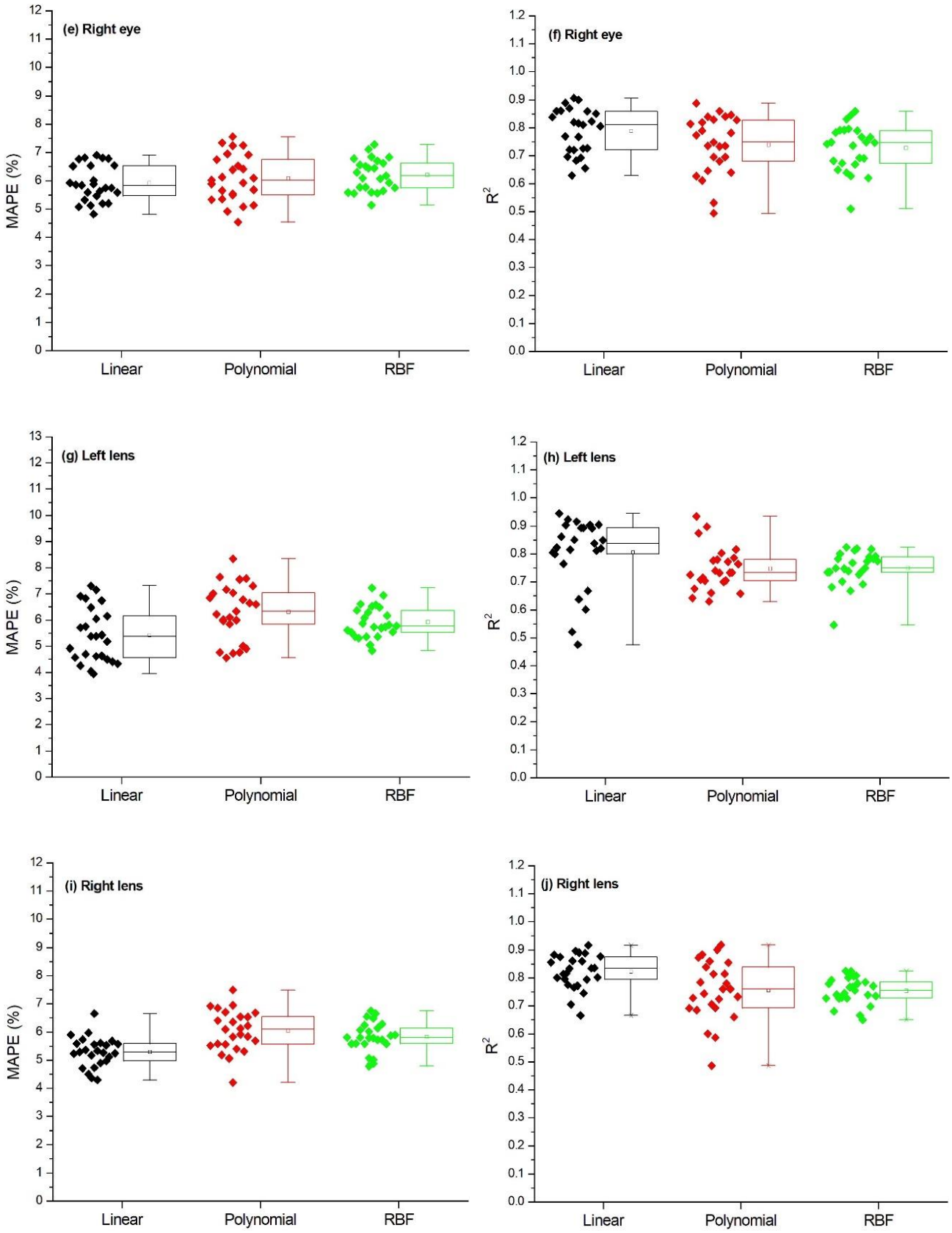

Figure 2. *Regression metrics of the SVR models with linear, polynomial, and RBF kernels for the investigated head organs including the brain's MAPE (a), brain's R^2 (b), left eye's MAPE (c), left eye's R^2 (d), right eye's MAPE (e), right eye's R^2 (f), left lens' MAPE (g), left lens' R^2 (h), right lens' MAPE (e), right lens' R^2 (f).*

As plotted in Figures 2c and 2d, the left eye exhibited mean MAPE values of 5.3%, 5.5%, and 5.8% across 25 random sample splits, with corresponding mean R^2 values of 0.8, 0.76, and 0.75 for the linear, polynomial, and RBF kernels. This implies that the SVR-based model with the linear kernel excels the overall performance among the three kernels when predicting patient-specific brain doses. In Figure 2d, few data points of low R^2 (<0.5) were also observed, which suggests the necessity to conduct R^2 robustness among different sample splits to get rid of ineffective sample splits. As illustrated in Figures 1e-1j, similar to the brain and left eye, linear kernel-based SVR achieved better overall performance for the right eye, left lens, and right lens as well. Thus, to maximize SVR's overall performance, the linear kernel could be applied to predict head organs in presence of R^2 robustness assessments.

3.2. Regression Metrics for the Abdominal Organs

Displayed in Figures 3a and 3b are the computed regression metrics for the bowel, revealing mean MAPE values of 6.4%, 6.7%, and 6.3% across 25 random sample splits for the linear, polynomial, and RBF kernels, respectively. Correspondingly, mean R^2 values were observed to be 0.85, 0.84, and 0.81 for linear, polynomial, and RBF kernels, respectively. The SVR-based model trained with the polynomial kernel exhibits better accuracy and generality when predicting bowel doses. For the bowel, it is suggested to evaluate the robustness in R^2 for the linear kernel across different patient sample splits, dismissing those with inferior regression metrics and identifying appropriate sample splits.

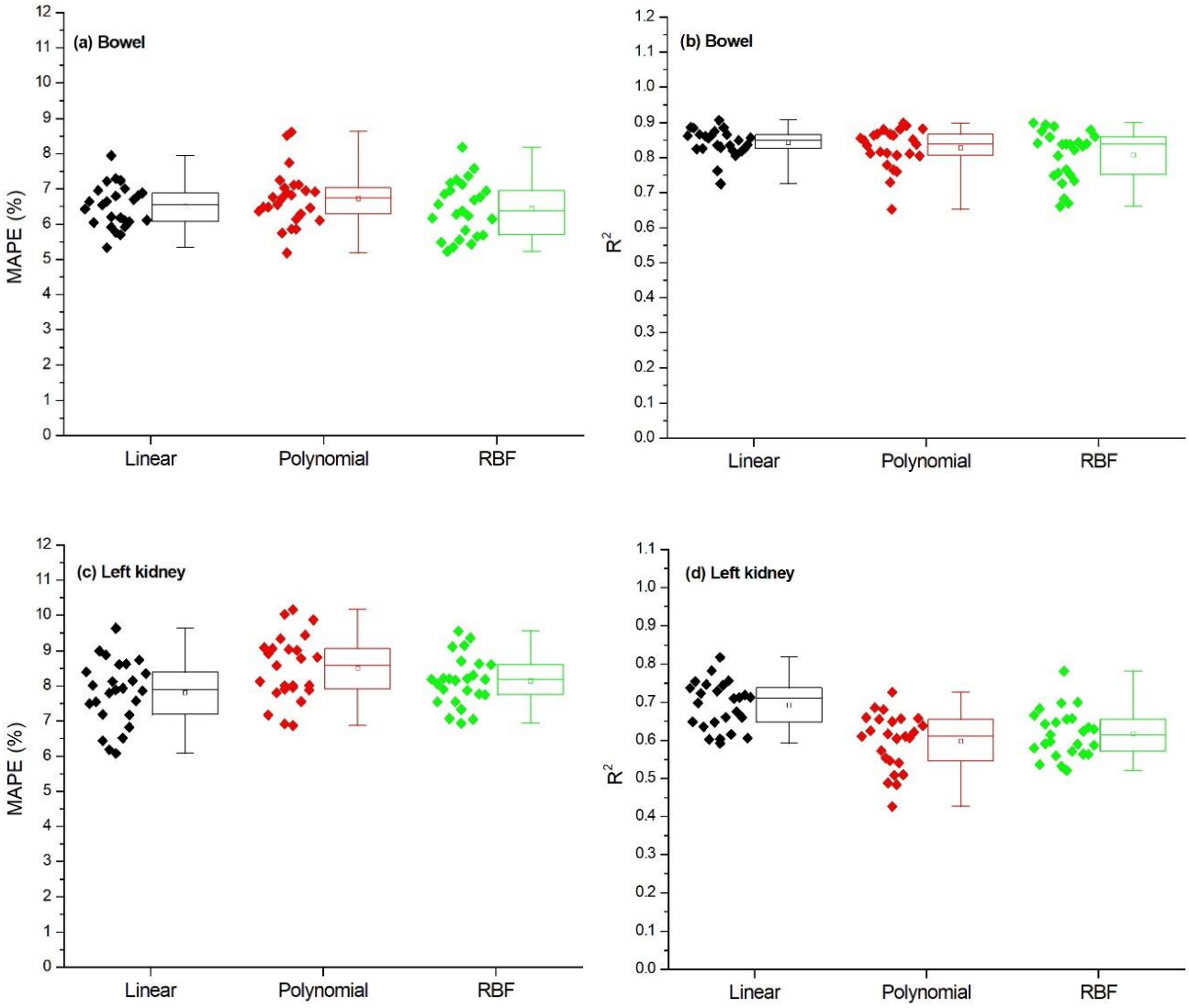

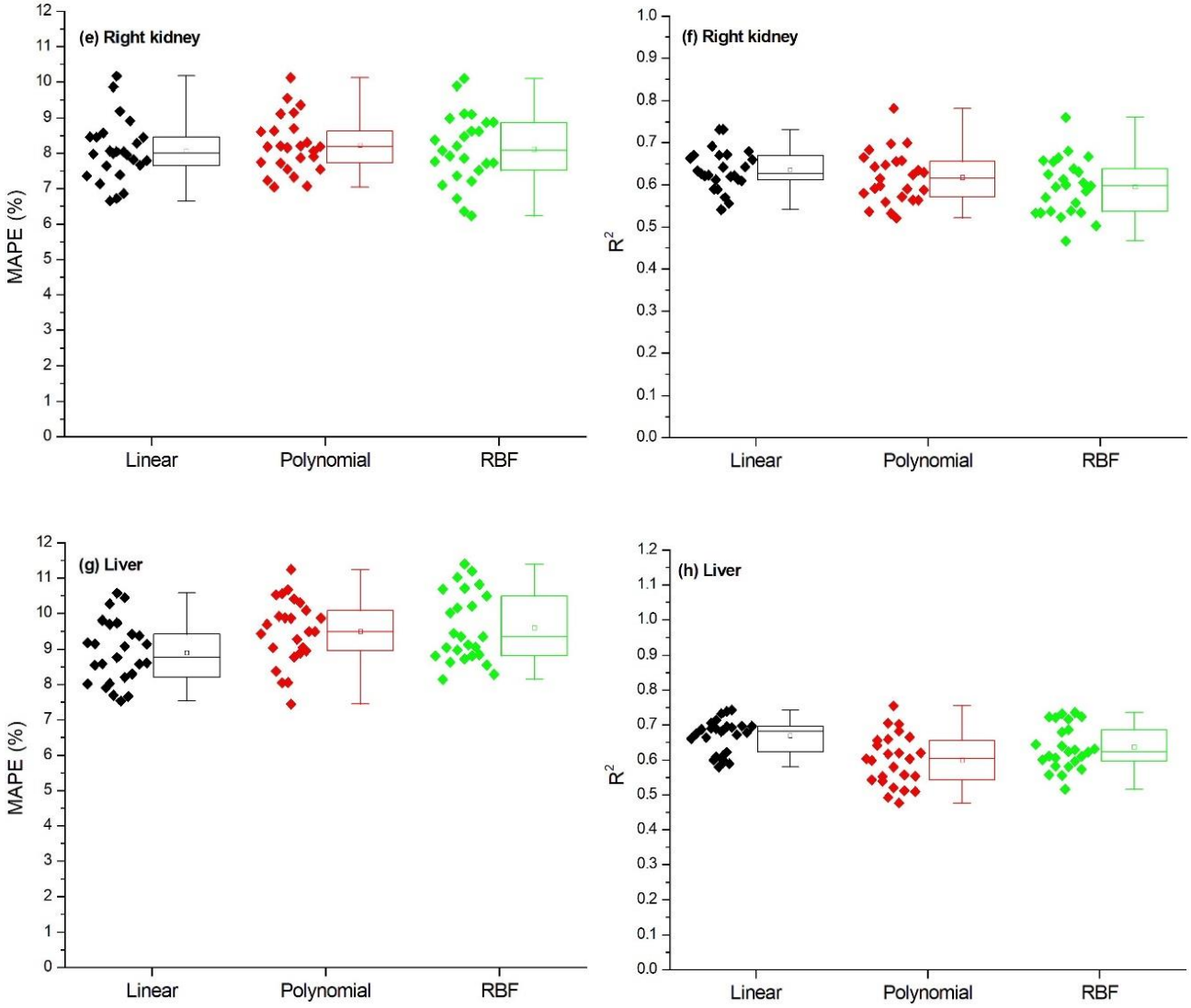

Figure 3. *Regression metrics of the SVR models with linear, polynomial, and RBF kernels for the investigated organs including the bowel' MAPE (a), bowel's R^2 (b), left kidney's MAPE (c), left kidney's R^2 (d), right kidney's MAPE (e), right kidney's R^2 (f), liver's MAPE (g), liver's R^2(h).*

In Figures 3c and 3d, the left kidney displays the mean MAPE values of 7.5%, 8.4%, and 7.7%, accompanied by mean R^2 values of 0.68, 0.61, and 0.6 for linear, polynomial, and RBF kernels, respectively. This suggests that the SVR-based model with the linear kernel outperformed the other kernels when predicting patient-specific brain doses. Thus, the linear kernel makes the SVR achieve the best overall performance for the left kidney. As illustrated in Figures 2e-2j, similar to the bowel and left kidney, the linear kernel-based SVR demonstrates superior overall performance for the right kidney and liver.

4. Discussion

Ionizing radiation emitted during CT scans exposes patients' organs, potentially increasing the risk of cancers to individuals underwent CT examinations. Developing SVR models based on radiomics features has proven to be an effective strategy for rapidly predicting patient-specific organ doses from CT scans. However, the previous study neglected kernel function selection, a crucial factor in maximizing SVR's predictive potential. Therefore, it is essential to explore SVR's predictive capabilities and further enhance the performance in predicting patient-specific organ doses. In recognition of the limitations of the previous study, this research applied linear, polynomial, and RBF kernels to construct SVR-based organ dose prediction models for each investigated organ. The goal is to pinpoint the optimal kernel function type for each organ.

To date, the previous study has adopted the RBF kernel to train SVR-based organ dose prediction models for head organs such as eyes, lens, and brain. The results of previous studies show that the MAPE in prediction head organs using the RBF-based SVR model is lower than 6%, and the R^2 larger than 0.7, suggesting satisfied performance in predictive ac-

curacy, generality, and robustness. However, the results of this study reveal that the linear could make the SVR achieve better overall performance than the RBF kernel for the brain, eyes, and lens. For the bowel, linear kernel exhibited better overall performance than RBF and polynomial kernels. Thus, kernel selection should be deemed as a required step when train SVR models based on radiomics features to predict head and abdominal organ doses. This is essential to maximize the predictive potential SVR-based models.

This research has certain limitations that should be acknowledged. Firstly, this kernel function selection study primarily focused on the CT scans of adult brains and abdomens, necessitating the development of a specialized prediction model for personalized organ doses in pediatric cases using the proposed SVR method. Secondly, we exclusively investigated five head organs (i.e. brain, left eye, right eye, left lens, right lens) and four abdominal organs (i.e. bowel, left kidney, right kidney, liver). Thus, the results of this study are mainly applicable to the nine investigated organs. It is still necessary to study other organs beyond the nine investigated organs, because organ type significantly impacts the kernel selection. Additionally, the proficiency of the optimized SVR model with the optimal kernel in predicting patient-specific organ doses was established in patients undergoing brain and abdominal CT scans at only one institution. However, to effectively apply this method elsewhere, different institutions need to train and optimize a new, institution-specific SVR model, taking into account their unique CT scanning parameters.

5. Conclusions

In this study, we optimized SVR models for patient-specific organ dose prediction from CT scans by conducting kernel function selection among the linear, polynomial, and RBF. The optimal kernel function significantly depends on organ types and CT scanned parts. Results show that the linear kernel achieves better overall performance in both accuracy (MAPE) and generality (R^2) than the polynomial and RBF kernels for most of the head and abdominal organs. Thus, it is essential to perform the organ-specific kernel function through kernel selection process to make use of SVR' predictive potential in predicting patient-specific organ doses from CT scans as much as possible while ensuring accuracy, generalizability, and robustness.

Abbreviations

SVR	Support Vector Regression
MAPE	Mean Absolute Percentage Error
R^2	R-squared
RBF	Radial Basis Function
IQR	Interquartile Range
ROI	Regions of Interest

Acknowledgments

The authors declare no conflicts of interest. Special thanks are extended to Professor George X. Xu and his group for providing technical support in the auto-segmentation of ROIs using DeepViewer.

Ethics

This research adhered to the Declaration of Helsinki guidelines. Utilizing available CT data from our hospital, we conducted a retrospective study approved by the hospital administration for research purposes. The study strictly adhered to the ethical guidelines of the hospital, ensuring anonymization of CT data and safeguarding personal information.

Author Contributions

Wencheng Shao: Conceptualization, Data curation, Formal Analysis, Investigation, Methodology, Software, Validation, Visualization, Writing – original draft

Xin Lin: Data curation, Formal Analysis, Investigation, Software, Validation, Writing – review & editing

Ying Hunag: Conceptualization, Methodology, Software, Writing – review & editing

Liangyong Qu: Data curation, Formal Analysis, Resources, Writing – review & editing

Weihai Zhuo: Conceptualization, Funding acquisition, Methodology, Project administration, Resources, Supervision, Writing – review & editing

Haikuan Liu: Conceptualization, Funding acquisition, Methodology, Project administration, Resources, Supervision, Writing – review & editing

Funding

Funding for this study was provided by the National Natural Science Foundation of China (Grant No. 12075064) and the National Key R&D Program of China (Grant No. 2019YFC0117254).

Conflicts of Interest

The authors declare no conflicts of interest.

References

[1] Hussain, S., Mubeen, I., Ullah, N., Shah, S. S. U. D., Khan, B. A., Zahoor, M., Ullah, R., Khan, F. A. and Sultan, M. A., 2022. Modern Diagnostic Imaging Technique Applications and Risk Factors in the Medical Field: A Review. BioMed research international, 2022, p. 5164970.

[2] Abhisheka, B., Biswas, S. K., Purkayastha, B., Das, D. and Escargueil, A., 2023. Recent trend in medical imaging modalities and their applications in disease diagnosis: a review. Multimedia Tools and Applications, pp. 1-36.

[3] Yitbarek, D. and Dagnaw, G. G., 2022. Application of advanced imaging modalities in veterinary medicine: a review. Veterinary Medicine: Research and Reports, pp. 117-125.

[4] Furlani, M., Riberti, N., Gatto, M. L. and Giuliani, A., 2023. High-Resolution Phase-Contrast Tomography on Human Collagenous Tissues: A Comprehensive Review. Tomography, 9(6), pp. 2116-2133.

[5] Spinnato, P., Patel, D. B., Di Carlo, M., Bartoloni, A., Cevolani, L., Matcuk, G. R. and Crombé, A., 2022. Imaging of Musculoskeletal Soft-Tissue Infections in Clinical Practice: A Comprehensive Updated Review. Microorganisms, 10(12), p. 2329.

[6] Addala, D. N., Denniston, P., Sundaralingam, A. and Rahman, N. M., 2023. Optimal diagnostic strategies for pleural diseases and identifying high-risk patients. Expert Review of Respiratory Medicine, 17(1), pp. 15-26.

[7] Hines Jr, J. J., Mikhitarian, M. A., Patel, R. and Choy, A., 2021. Spectrum and relevance of incidental bowel findings on computed tomography. Radiologic Clinics, 59(4), pp. 647-660.

[8] Jain, S., 2021. Radiation in medical practice & health effects of radiation: Rationale, risks, and rewards. Journal of Family Medicine and Primary Care, 10(4), p. 1520.

[9] Shao, Y. H., Tsai, K., Kim, S., Wu, Y. J. and Demissie, K., 2020. Exposure to tomographic scans and cancer risks. JNCI cancer spectrum, 4(1), p. pkz072.

[10] Foucault, A., Ancelet, S., Dreuil, S., Caer-Lorho, S., Ducou Le Pointe, H., Brisse, H., Chateil, J. F., Lee, C., Leuraud, K. and Bernier, M. O., 2022. Childhood cancer risks estimates following CT scans: an update of the French CT cohort study. European Radiology, 32(8), pp. 5491-5498.

[11] Farkouh, A. A. and Baldwin, D. D., 2023. Radiation Hazards in Endourology. In Percutaneous Renal Surgery (pp. 121-141). Cham: Springer International Publishing.

[12] Maier, J., Eulig, E., Dorn, S., Sawall, S. and Kachelrieß, M., 2018, November. Real-time patient-specific CT dose estimation using a deep convolutional neural network. In 2018 IEEE Nuclear Science Symposium and Medical Imaging Conference Proceedings (NSS/MIC) (pp. 1-3). IEEE.

[13] Xie, T. and Zaidi, H., 2019. Estimation of the radiation dose in pregnancy: an automated patient-specific model using convolutional neural networks. European radiology, 29, pp. 6805-6815.

[14] Imran, A. A. Z., Wang, S., Pal, D., Dutta, S., Patel, B., Zucker, E. and Wang, A., 2021. Personalized CT organ dose estimation from scout images. In Medical Image Computing and Computer Assisted Intervention–MICCAI 2021: 24th International Conference, Strasbourg, France, September 27–October 1, 2021, Proceedings, Part IV 24 (pp. 488-498). Springer International Publishing.

[15] Tzanis E, Damilakis J. A novel methodology to train and deploy a machine learning model for patient-specific dose assessment in head CT. Eur Radiol. 2022; 32(9): 6418-6426.

[16] Christner, J. A., Braun, N. N., Jacobsen, M. C., Carter, R. E., Kofler, J. M. and McCollough, C. H., 2012. Size-specific dose estimates for adult patients at CT of the torso. Radiology, 265(3), pp. 841-847.

[17] Moore, B. M., Brady, S. L., Mirro, A. E. and Kaufman, R. A., 2014. Size‐specific dose estimate (SSDE) provides a simple method to calculate organ dose for pediatric CT examinations. Medical physics, 41(7), p. 071917.

[18] Franck, C., Vandevoorde, C., Goethals, I., Smeets, P., Achten, E., Verstraete, K., Thierens, H. and Bacher, K., 2016. The role of Size-Specific Dose Estimate (SSDE) in patient-specific organ dose and cancer risk estimation in paediatric chest and abdominopelvic CT examinations. European radiology, 26, pp. 2646-2655.

[19] Brink, J. A. and Morin, R. L., 2012. Size-specific dose estimation for CT: how should it be used and what does it mean?. Radiology, 265(3), pp. 666-668.

[20] Maior, C. B., Santana, J. M., Lins, I. D. and Moura, M. J., 2021. Convolutional neural network model based on radiological images to support COVID-19 diagnosis: Evaluating database biases. Plos one, 16(3), p. e0247839.

[21] Park, D. J., Park, M. W., Lee, H., Kim, Y. J., Kim, Y. and Park, Y. H., 2021. Development of machine learning model for diagnostic disease prediction based on laboratory tests. Scientific reports, 11(1), p. 7567.

[22] Jeyaraman, M., Balaji, S., Jeyaraman, N. and Yadav, S., 2023. Unraveling the ethical enigma: Artificial intelligence in healthcare. Cureus, 15(8).

[23] Murphy, K., Di Ruggiero, E., Upshur, R., Willison, D. J., Malhotra, N., Cai, J. C., Malhotra, N., Lui, V. and Gibson, J., 2021. Artificial intelligence for good health: a scoping review of the ethics literature. BMC medical ethics, 22(1), pp. 1-17.

[24] Drucker, H., Burges, C. J., Kaufman, L., Smola, A., & Vapnik, V. N. (1996). Support Vector Regression Machines. Neural Information Processing Systems.

[25] Chih-Cheng Yang, Wan-Jui Lee and Shie-Jue Lee, "Learning of Kernel Functions in Support Vector Machines," The 2006 IEEE International Joint Conference on Neural Network Proceedings, Vancouver, BC, Canada, 2006, pp. 1150-1155, https://doi.org/10.1109/IJCNN.2006.246820

[26] Shao W, Xin L, Yi Y, Huang Y, Qu L, Zhuo W, Liu H. Fast prediction of patient-specific organ doses in brain CT scans using support vector regression algorithm. Phys Med Biol. 2023 Dec 12. https://doi.org/10.1088/1361-6560/ad14c7 Epub ahead of print.

[27] Peng Z, Chang YK, Song YC, et al. Validation and Clinical Application of DL-Based Automatic Target and OAR Segmentation Software, DeepViewer. In: Proceedings of the American Association of Physicists in Medicine Annual Meeting (Vancouver, BC, July 12-16). 2020: 123-124.

[28] Thomas Phil, Thomas Albrecht, Skylar Gay, & Mathis Ersted Rasmussen. (2023). Sikerdebaard/dcmrtstruct2nii: dcmrtstruct2nii v5 (Version v5). Zenodo. Available from: https://github.com/Sikerdebaard/dcmrtstruct2nii

[29] van Griethuysen JJM et al. Computational radiomics system to decode the radiographic phenotype. Cancer Res 2017; 77: e104-e107.

[30] Rebuffi S-A, Gowal S, Calian DA, et al. Data Augmentation Can Improve Robustness. In: Advances in Neural Information Processing Systems 34 (NeurIPS 2021). Neural Information Processing Systems Foundation; 2021: 1234-1245.

[31] Zhang, J. and Wang, X., 1997. Selecting the best regression equation via the P-value of F-test. Metrika, 46, pp. 33-40.

[32] Anaconda | The World's Most Popular Data Science Platform. https://www.anaconda.com/ Accessed January 28, 2022.

[33] Bert J et al. GGEMS: GPU GEant4-based Monte Carlo Simulation platform. In: Proceedings of the IEEE Nuclear Science Symposium and Medical Imaging Conference (NSS/MIC). IEEE; 2016: 1234-1245.